Journal of Pain Research

Dovepress
open access to scientific and medical research

Open Access Full Text Article

ORIGINAL RESEARCH

Ligusticum chuanxiong Hort. Ameliorates Neuropathic Pain by Regulating Microglial M1 Polarization: A Study Based on Network Pharmacology

Shanshan Cui[1], Xiaobo Feng[2], Zhongyuan Xia[1]

[1]Department of Anesthesiology, Renmin Hospital of Wuhan University, Wuhan, Hubei Province, People's Republic of China; [2]Department of Anesthesiology, Zhongnan Hospital, Wuhan University, Wuhan, Hubei Province, People's Republic of China

Correspondence: Zhongyuan Xia, Department of Anesthesiology, Renmin Hospital of Wuhan University, Ziyang Road, Wuchang District, Wuhan, Hubei Province, People's Republic of China, Email xiazhongyuan2005@aliyun.com

Background: In traditional Chinese medicine, *Ligusticum chuanxiong Hort*. (LCH) is used to treat neuropathic pain (NP). This study was performed to investigate the underlying pharmacological mechanisms.

Methods: The main components of the LCH were obtained from the TCMSP database. The targets of the active components were obtained using the Swiss Target Prediction database and HERB database. The NP-related genes were obtained from the CTD database and GeneCard database. Protein-protein interaction (PPI) network was constructed using the STRING platform and Cytoscape 3.9.0 software. GO and KEGG enrichment analyses were performed using the DAVID database. Interactions between the key components and hub target proteins were verified using molecular docking and molecular dynamics simulation. In addition, microglial cell line HMC3 was induced to polarize to the M1 phenotype using 100 ng/mL lipopolysaccharide (LPS). Quantitative real-time polymerase chain reaction (qRT-PCR), Western blot and enzyme-linked immunosorbent assays were used to detect the expression levels of M1 markers and inflammatory factors, respectively.

Results: Seven LCH active components of LCH were identified, corresponding to 387 target genes. 2019 NP-related genes were obtained, and a total of 174 NP-related genes were identified as target genes that could be modulated by LCH. Beta-sitosterol, senkyunone, wallichilide, myricanone, and mandenol were considered as the key components of LCH in the treatment of NP. SRC, BCL2, AKT1, HIF1A and HSP90AA1 were identified as the hub target proteins. GO analysis showed that 328 biological processes, 61 cell components, and 85 molecular functions were likely modulated by the components of LCH, and KEGG enrichment analysis showed that 132 signaling pathways were likely modulated by the components of LCH. Beta-sitosterol, senkyunone, wallichilide, myricanone, and mandenol showed good binding activity with hub target proteins including SRC, BCL2, AKT1, and HSP90AA1. In addition, beta-sitosterol inhibited LPS-induced M1 polarization in HMC3 in vitro.

Conclusion: This study provides a theoretical basis for the application of LCH in the treatment of NP through multicomponent, multitarget, and multiple pathways.

Keywords: neuropathic pain, *Ligusticum chuanxiong Hort*., network pharmacology, molecular docking, microglia, inflammation

Introduction

Neuropathic pain (NP) is a type of chronic pain caused by damage to the peripheral or central nervous system,[1] mainly manifests as spontaneous pain, hyperalgesia, dysalgesia, and secondary hyperalgesia.[2] It is estimated that 11–40% of adults suffer from chronic pain.[3] NP often leads to sleep disorders and even depression in patients, which seriously affects the quality of life of patients.[4,5] However, traditional treatments for NP are still limited to nonsteroidal anti-inflammatory drugs, antidepressants, antiepileptics, opioid analgesics and local anesthetics.[6,7] These drugs are often insufficient to relieve NP and often have many serious side effects. Therefore, there is an urgent need to explore NP therapeutic drugs with a definite efficacy and minimal side effects.

Received: 8 November 2023
Accepted: 9 May 2024
Published: 23 May 2024

Ligusticum chuanxiong Hort. (LCH), belonging to the Umbelliferae family, is a widely used medicinal and edible plant. In China, LCH is often used to treat gynecological diseases, such as dysmenorrhea, amenorrhea, dystocia and lochia,[8,9] and it is also applied to treat ischemic diseases, such as dizziness, headache and migraine.[10–12] To date, more than 263 bioactive substances have been isolated from different parts of LCH (rhizomes, fibrous roots, and aboveground parts), including volatile oils, organic acids, phenolic acids, phthalates, alkaloids, polysaccharides, ceramides, cerebrosides and terpenoids.[12] Modern pharmacological studies have shown that LCH has analgesic, anti-inflammatory, antioxidant, antitumor, anti-coagulation, anti-depression, anti-aging, anti-atherosclerosis, and improving cardiac function effects.[13–16] However, its potential function and mechanism of action in the treatment of NP remain unclear.

Network pharmacology is a promising approach that uses bioinformatics and pharmacology to reveal interactions between traditional Chinese medicine (TCM) and diseases.[17] This study was performed to explore the potential active components of LCH using network pharmacology and to investigate its potential function and mechanism in the treatment of NP. In addition, we verified the regulatory effects of beta-sitosterol on the M1 phenotypic switch of microglia induced by lipopolysaccharide (LPS).

Materials and Methods

Screening of LCH Active Components and Their Action Targets

The TCMSP database (https://www.tcmsp-e.com/) was used to determine the composition of the LCH. TCM is mostly administered orally, and acts on organs and tissues after absorption, distribution, metabolism and excretion (ADME) in the body, playing a variety of biological roles, which is called TCM pharmacokinetics. Oral bioavailability (OB) and drug-likeness (DL) are important parameters of ADME.[18] In this study, OB≥30% and DL≥0.18 were selected as the standards for the main candidate bioactive components. In addition, PubChem (https://pubchem.ncbi.nlm.nih.gov/) was searched for SMILES files. The Swiss Target Prediction database (http://www.swisstargetprediction.ch/; probability>0) and HERB database (http://herb.ac.cn/) were searched for potential targets of the bioactive components of LCH.

Screening and Collection of NP-Related Genes

With "neuropathic pain" as the search term, Comparative Toxicogenomics Database (CTD) (https://ctdbase.org/; Inference Score 30 or higher)[19] and GeneCards (https://www.genecards.org/; Relevance score≥1)[20] predicted NP disease targets. After integrating the retrieved targets and deleting duplicate values, NP-related targets were obtained.

Screening Core Components of LCH in Treating NP

The targets of LCH components and NP-related targets were input into the Venn online platform (https://www.bioladder.cn/web/#/chart/17) to map the Venn graph and obtain the intersection of two sets of targets. Then, Cytoscape 3.9.0 software was used to construct the "drug - active component - intersection target - disease" network diagram, and CytoNCA plug-in was used to calculate the degree value of network nodes to screen out the core components of LCH.

Construction and Analysis of Protein-Protein Interaction (PPI) Network

A PPI network of common targets was constructed using the STRING database (https://cn.string-db.org/) to explore core targets. The species was set to "Homo Sapiens", and the required minimum interaction score was set to High Confidence (0.7). The PPI network diagram was obtained after removing the free points and the TSV file was downloaded and saved. The MCODE plug-in was used for the cluster analysis of the PPI networks. The parameters were set as follows: degree cutoff=2, node score cutoff=0.2, K-score=2, and maximum depth=100. In addition, the CytoHubba plugin was used to calculate seven different parameters, including betweenness, closeness, edge percolated component (EPC), degree, maximum neighborhood component (MNC), radiality, and stress, to obtain the top 10 key genes in the PPI network and to further screen out the hub genes. The results were visualized using R package ggraph and UpSetR.

Gene Ontology (GO) and Kyoto Encyclopedia of Genes and Genomes (KEGG) Enrichment Analyses

The DAVID database (https://david.ncifcrf.gov/tools.jsp) was used for GO and KEGG pathway enrichment analyses. The species was limited to "Homo Sapiens", and the related biological functions / processes and signaling pathways of LCH in NP treatment were obtained with $P<0.01$ as the screening condition. The top 30 KEGG items with the lowest P value were imported into Cytoscape 3.9.0 software to plot the pathway-target network diagram.

Molecular Docking

Molecular docking was performed using the AutoDock Vina software (version 1.1.2). X-ray crystal structures of the hub target proteins were obtained from the Protein Data Bank (PDB) database (https://www.rcsb.org/). The PyMOL software was used to remove H_2O molecules from the protein crystal structure, add hydrogen atoms, and calculate the charge. PubChem (https://pubchem.ncbi.nlm.nih.gov/) was searched to download the 2D structure of the key components, and the documents were saved in the SDF format and transformed into mol2 format using OpenBabel software (version 3.1.1). AutoDockTools1.5.7 software was used to convert all protein and molecular ligand files into the PDBOT format. Subsequently, molecular docking was performed using AutoDock Vina (version 1.1.2) to calculate binding energy. The docking results were visualized using PyMOL software v.2.4.0.

Microglia Culture

Microglial HMC3 cells were purchased from American Type Culture Collection (ATCC, Manassas, VA, USA). The cells were cultured in Dulbecco's Modified Eagle's medium (DMEM; Invitrogen, Carlsbad, CA, USA) containing 10% fetal bovine serum (FBS; Gibco, Rockville, MD, USA), 100 U/mL penicillin, and 100 μg/mL streptomycin (Gibco, Rockville, MD, USA), in a humidified incubator at 37 °C in 5% CO_2. As previously reported,[21] to induce M1 polarization of HMC3 cells, the cells were treated with 100 ng/mL LPS for 24 h. HMC3 cells treated with phosphate-buffered saline (PBS) for 24 h were used as the control. To study the toxicity of beta (β) -sitosterol (95% purity, Cas No. 83-46-5; Sigma-Aldrich, Shanghai, China), HMC3 cells were treated with β-sitosterol at different concentrations (0, 7.5, 15, 30, and 60 μM) for 24 h. To investigate the effect of β-sitosterol on M1 polarization of HMC3 cells, the cells were treated with β-sitosterol (30 or 60 μM) and 100 ng/mL LPS for 24 h.

Cell Viability Assay

Cell viability was detected by Cell Counting Kit-8 (CCK-8) (Beyotime Biotechnology, Shanghai, China). Briefly, HMC3 cells were seeded in 96-well plates at a density of 5×10^3 cells/well and incubated for 24 h. Then, 10 μL of CCK-8 solution was added to each well and the plates were incubated at 37 °C for 2 h. Finally, the optical density (OD) was measured using a microplate reader (Dynatech Labs, Chantilly, VA, USA) at 450 nm and cell viability was calculated.

Quantitative Real-Time Polymerase Chain Reaction (qRT-PCR)

Total RNA was extracted using TRIzol reagent (Invitrogen, Carlsbad, CA, USA) according to the manufacturer's instructions. Total RNA (800 ng) was reverse-transcribed into complementary DNA (cDNA) using the M-MLV Reverse Transcription Kit (Promega, Shanghai, China). qRT-PCR was performed using the Power SYBR Green PCR Master Mix kit (Applied Biosystems, Foster City, CA, USA). β-actin was used as an endogenous control, and the relative expression of the target gene was calculated by $2^{-\Delta\Delta Ct}$ method. The primers used in this study were shown in Table 1.

Western Blot

The treated HMC3 cells were collected and lysed in RIPA buffer containing protease inhibitors (Sigma, St. Louis, MO, USA), and the total cell protein was harvested. Protein was quantified using a BCA kit (Beyotime, Shanghai, China). After separating 30 μg of protein on 12% sodium dodecyl sulfate-polyacrylamide gel for 2 h, the protein were transferred to a polyvinylidene difluoride (PVDF) membrane (Millipore, Billerica, MA, USA). Then, the membrane was blocked with 5% skim milk at room temperature for 2h. Then the membranes were incubated with the primary antibodies at 4 °C

Table 1 Sequences for qRT-PCR Primers

Name	Primer Sequences
iNOS	Forward: 5'-GGAAGAGGAACAACTACTGCTGGT-3'
	Reverse: 5'-GAACTGAGGGTACATGCTGGAGC-3'
CD86	Forward: 5'-AGGAGCCTTAGGAGGTACGG-3'
	Reverse: 5'-AATCAAAACTTGTGCGGCCC-3'
COX-2	Forward: 5'-TTCTCTCGGTTAGCGACCAATT-3'
	Reverse: 5'-CTGAGGGCGTCTGGCTGT-3'
TNF-α	Forward: 5'-GACAAGCCTGTAGCCCATGT-3'
	Reverse: 5'-GGAGGTTGACCTTGGTCTGG-3'
IL-6	Forward: 5'-CCACCGGGAACGAAAGAGAA-3'
	Reverse: 5'-GAGAAGGCAACTGGACCGAA-3'
IL-1β	Forward: 5'-CAGAAGTACCTGAGCTCGCC-3'
	Reverse: 5'-TGAAGCCCTTGCTGTAGTGG-3'
SRC	Forward: 5'-CCCTTTCCCCTCTAGCCTCA-3'
	Reverse: 5'-GGAGTGAACATGGCCACAGA-3'
BCL2	Forward: 5'-AAAAATACAACATCACAGAGGAAGT-3'
	Reverse: 5'-TCCCGGTTATCGTACCCTGT-3'
AKT1	Forward: 5'-CAAGGTGATCCTGGTGAA-3'
	Reverse: 5'-CGTGGGTCTGGAAAGAGT-3'
HIF1A	Forward: 5'-AGAGGTTGAGGGACGGAGAT-3'
	Reverse: 5'-CTCCGACATTGGGAGCTCAT-3'
HSP90AA1	Forward: 5'-AGGAGGTTGAGACGTTCGC-3'
	Reverse: 5'-AGAGTTCGATCTTGTTTGTTCGG-3'
β-actin	Forward: 5'-CCCTGGACTTCGAGCAAGAG-3'
	Reverse: 5'-AATGCCAGGGTACATGGTGG-3'

for 1 h. The primary antibodies included anti-inducible nitric oxide synthase (iNOS) antibody (ab178945, 1:1000, Abcam), anti-CD86 antibody (ab239075, 1:1000, Abcam), anti-cyclooxygenase 2 (COX-2) antibody (ab179800, 1:1000, Abcam), anti-tumor necrosis factor-α (TNF-α) antibody (ab183218, 1:1000, Abcam), anti-interleukin-6 (IL-6) antibody (ab233706, 1:1000, Abcam), anti-interleukin-1β (IL-1β) antibody (ab315084, 1:1000, Abcam), anti-AKT antibody (ab8805, 1:1000, Abcam), anti-PI3 Kinase (PI3K) p85 alpha (α) antibody (ab191606, 1:1000, Abcam), anti-mammalian target of rapamycin (mTOR) antibody (ab2732, 1:1000, Abcam), anti-phospho (p)-AKT (T308) antibody (ab38449, 1:1000, Abcam), anti-p-PI3K p85α (Y607) antibody (ab182651, 1:1000, Abcam), anti-p-mTOR (S2481) antibody (ab137133, 1:1000, Abcam), and anti-β-actin antibody (ab8227, 1:1000, Abcam). The membrane was then incubated with goat anti-rabbit IgG H&L (HRP) (ab205718, 1:5000, Abcam) at room temperature for 1 h. Protein bands were detected with a BeyoECL Plus kit (Beyotime, Shanghai, China). ImageLab software (version 4.1) (Bio-Rad Laboratories, Hercules, CA, USA) was used for image acquisition and density value analysis.

Enzyme-Linked Immunosorbent Assay (ELISA)

HMC3 cells were collected and centrifuged at 1000×g at 4 °C for 10 min to obtain the supernatant. Then, according to the manufacturer's instructions, the ELISA kits (R&D Systems Inc., Minneapolis, MN, USA) was used to detect the levels of TNF-α, IL-6 and IL-1β in the supernatant.

Molecular Dynamics Simulation

Desmond module of the Schordinger 2019 software was used to perform Molecular dynamics simulation in the TIP3P water model. OPLS2005 force field was used to simulate water molecules. In order to neutralize the system charge, an appropriate amount of chloride/sodium ions was added to balance the system charge and placed randomly in the solvation system. After the solvation system was constructed, the system was energy minimized. The Nose-Hoover temperature coupling and isotropic scale were used to maintain the temperature and pressure at 300 K and 1.013 bar

pressure. Subsequently, molecular dynamics trajectories were recorded every 100 ps intervals and simulations were lasted for 100 ns. Finally, root mean square deviation (RMSD) and root mean square fluctuation (RMSF) were calculated for all frames in the trajectory with respect to the reference frame.

Statistical Analysis

All experiments were independently conducted in triplicates. All data are expressed as "mean ± standard deviation (SD)". SPSS (version 21.0; IBM Corp., Armonk, NY, USA) was used for statistical analysis of the data. Multivariate comparisons were performed using one-way analysis of variance (ANOVA) and Tukey's post hoc test. $P < 0.05$ was considered statistically significant.

Results

Collection of Bioactive Components of LCH and Their Targets

According to the screening criteria of OB≥30% and DL≥0.18, 7 LCH active components were identified in the TCMSP database (Table 2). The chemical structures of the active components are shown (Figure 1). Swiss Target Prediction and HERB databases were used to predict potential targets for LCH active components, and 387 drug targets were obtained.

Collection of NP-Related Genes

In the GeneCards and CTD databases, 1429 and 823 NP-related disease target genes were identified, respectively, using the keyword "neuropathic pain". After merging and removing duplicate targets, 2019 NP-related disease targets were identified.

Target Screening and Network Construction of LCH in NP Treatment

To identify potential targets of LCH in treating NP, we cross-analyzed 387 drug targets with the 2019 NP-related genes. The results showed that 174 target genes in the intersection were identified as potential candidate target genes for the LCH in NP treatment (Figure 2A). The "drug-active component-intersection target-disease" network was then constructed using Cytoscape 3.9.0 software to further understand the correlation between LCH bioactive component targets and NP targets. The network consisted of 183 nodes and 456 edges (Figure 2B). The degree value of each node in the network was calculated using the CytoNCA plug-in. β-sitosterol, senkyunone, wallichilide, myricanone, and mandenol, with the highest degree values, were considered key components of LCH in NP treatment (Figure 2C).

PPI Network Construction

To investigate the potential mechanism of action of LCH in NP treatment, 174 target genes were imported into the STRING database to construct a PPI network. The network consisted of 173 nodes and 707 edges (Figure 3A). Furthermore, topological parameter analysis of the PPI network was performed using the CytoNCA plug-in in Cytoscape 3.9.0 software. All nodes were arranged in a circle according to the degree values; the larger the degree value, the larger the node, and the darker the color (Figure 3B). In addition, cluster analysis of PPI networks using the MCODE plug-in generated six gene clusters associated with LCH in NP treatment (Figure 3C and Table 3). Cluster 1 had the highest score and contained 15 nodes and 70 edges.

Identification of Hub Genes

The top ten key genes of the PPI network were obtained using the CytoHubba plug-in through seven different algorithms (betweenness, closeness, EPC, degree, MNC, radiality, and stress) (Figure 4A). Furthermore, cross-analysis of the results of the seven calculation methods showed that SRC, BCL2, AKT1, HIF1A, and HSP90AA1 were hub genes of the PPI network (Figure 4B and C). Detailed information on the five hub genes is provided in Table 4.

Table 2 Details of Active Compounds in Ligusticum Chuanxiong Hort

Mol ID	Molecule Name	OB (%)	DL	PubChem cid	Molecule Smile	Swiss Target Prediction	HERB	Total	Molecular Formula
MOL001494	Mandenol	42	0.19	5282184	CCCCCC=CCC=CCCCCCCCC(=O)OCC	108	6	111	C20H36O2
MOL002135	Myricanone	40.6	0.51	161748	COC1=C2C=C(CCCCC(=O)CCC3=CC2=C(C=C3)O)C(=C1OC)O	102	23	121	C21H24O5
MOL002140	Perlolyrine	65.95	0.27	160179	C1=CC=C2C(=C1)C3=C(N2)C(=NC=C3)C4=CC=C(O4)CO	N/A	10	10	C16H12N2O2
MOL002151	Senkyunone	47.66	0.24	91726743	CC1=CC(=O)C=C(C1=O)CC=C(C)CCC=C(C)CCC=C(C)C	101	N/A	101	C22H30O2
MOL002157	Wallichilide	42.31	0.71	10873344	CCCCC(=O)C12CCC(C=C1C(=O)OC)C3C2C4=C(CC3)C(=CCCC)OC4=O	111	6	117	C25H32O5
MOL000359	Beta-Sitosterol	36.91	0.75	12303645	CCC(CCC(C)C1CCC2C1(CCC3C2CC=C4C3(CCC(C4)O)C)C)C(C)C	44	48	84	C29H50O
MOL000433	FA	68.96	0.71	6037	C1=CC(=CC=C1C(=O)NC(CCC(=O)O)C(=O)O)NCC2=CN=C3C(=N2)C(=O)N=C(N3)N	16	2	18	C19H19N7O6

Abbreviations: OB, oral bioavailability; DL, drug-likeness.

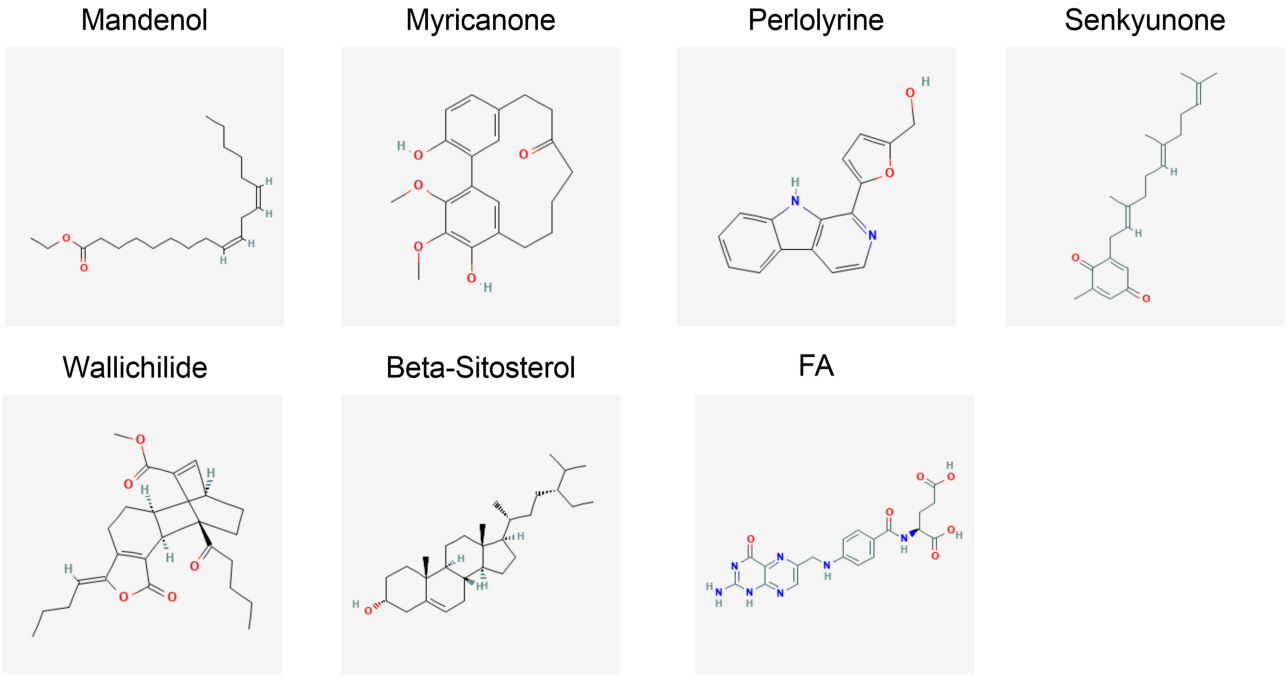

Figure 1 Chemical structure of 7 LCH active components.

Results of GO Analysis and KEGG Enrichment Analysis

A total of 474 GO enrichment terms were obtained ($P<0.01$), including 328 biological processes (BP), 61 cell components (CC), and 85 molecular functions (MF). The top 10 BP, CC, and MF terms with the highest gene counts were selected for visualization (Figure 5A–C). The top five BP items were signal transduction, protein phosphorylation, response to xenobiotic stimulus, inflammatory response, and intracellular signal transduction (Figure 5A). The top five CC items were the plasma membrane, cytosol, cytoplasm, integral components of the membrane, and nucleus (Figure 5B). The top five MF items were protein binding, identical protein binding, ATP-binding protein serine/threonine/tyrosine kinase activity, and protein kinase activity (Figure 5C). The top 10 BP, CC, and MF terms with the highest enrichment are shown in the bar chart (Figure 5D). In KEGG enrichment analysis, 132 pathways were found to be related to the mechanism of action of LCH in NP treatment. We then selected the top 30 KEGG pathways with the most enriched genes for visualization. The results showed that the target genes of LCH therapy for NP were mainly involved in pathways related to cancer (hsa05200), PI3K-Akt signaling pathway (hsa04151), neuroactive ligand-receptor interaction (hsa04080), calcium signaling pathway (hsa04020), human cytomegalovirus infection (hsa05163), Hepatitis B (hsa05161), Kaposi sarcoma-associated herpesvirus infection (hsa05167), chemical carcinogenesis, receptor activation (hsa05207), MAPK signaling pathway (hsa04010), and pathways of neurodegeneration and multiple diseases (hsa05022) (Figure 6A). The top 30 KEGG pathways were also categorized. These KEGG pathways fell into three main categories:, including environmental information processing (8 pathways), cellular processes (2 pathways), and human diseases (20 pathways) (Figure 6B). In addition, we conducted a secondary classification of all KEGG pathways (Figure 6C). In terms of metabolism, KEGG pathways were mainly associated with lipid metabolism and energy metabolism; in terms of cellular processes, these pathways were mainly enriched in cell growth and death, cellular community-eukaryotes, transport and catabolism, and cell motility.

Construction of Pathway-Target Network

The top 30 KEGG pathways and their related targets were imported into Cytoscape 3.9.0 software to construct the pathway-target network. As shown (Figure 7A), the network consisted of 145 nodes and 686 edges. Except for disease-specific signaling pathways (hsa05200 and hsa04080), the PI3K-AKT signaling pathway ranked first among the

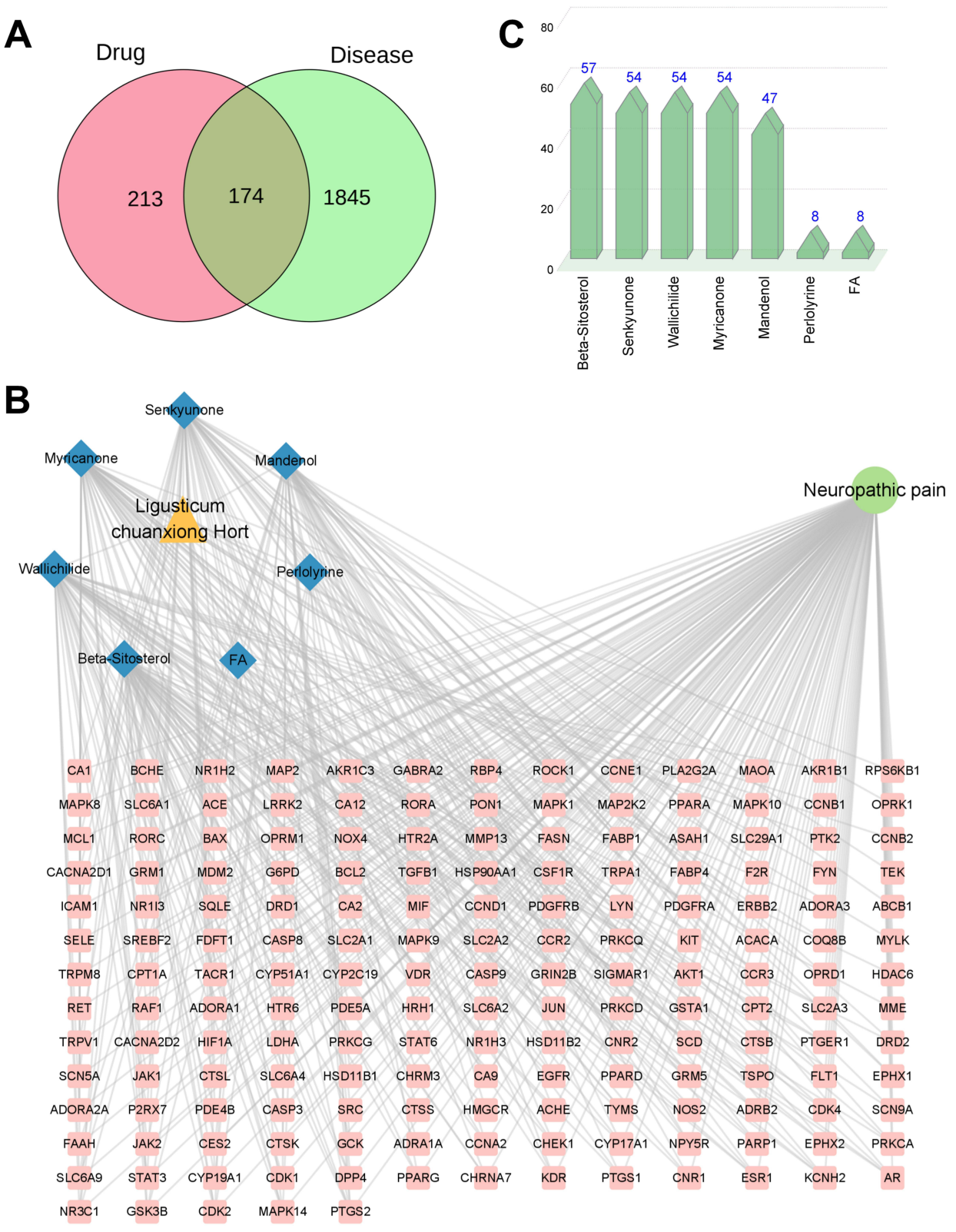

Figure 2 Screening the targets for LCH treatment of NP and network construction. (**A**) Venn diagram of the LCH target genes and NP-related genes. (**B**) The "LCH-active components-intersection target-NP" network diagram was constructed using Cytoscape 3.9.0 software. The green circular node represents the NP, yellow triangular node represents LCH, blue diamond node represents the seven active components of LCH, and pink rectangular node represents the intersection target. (**C**) Degree value statistics of 7 LCH active components.

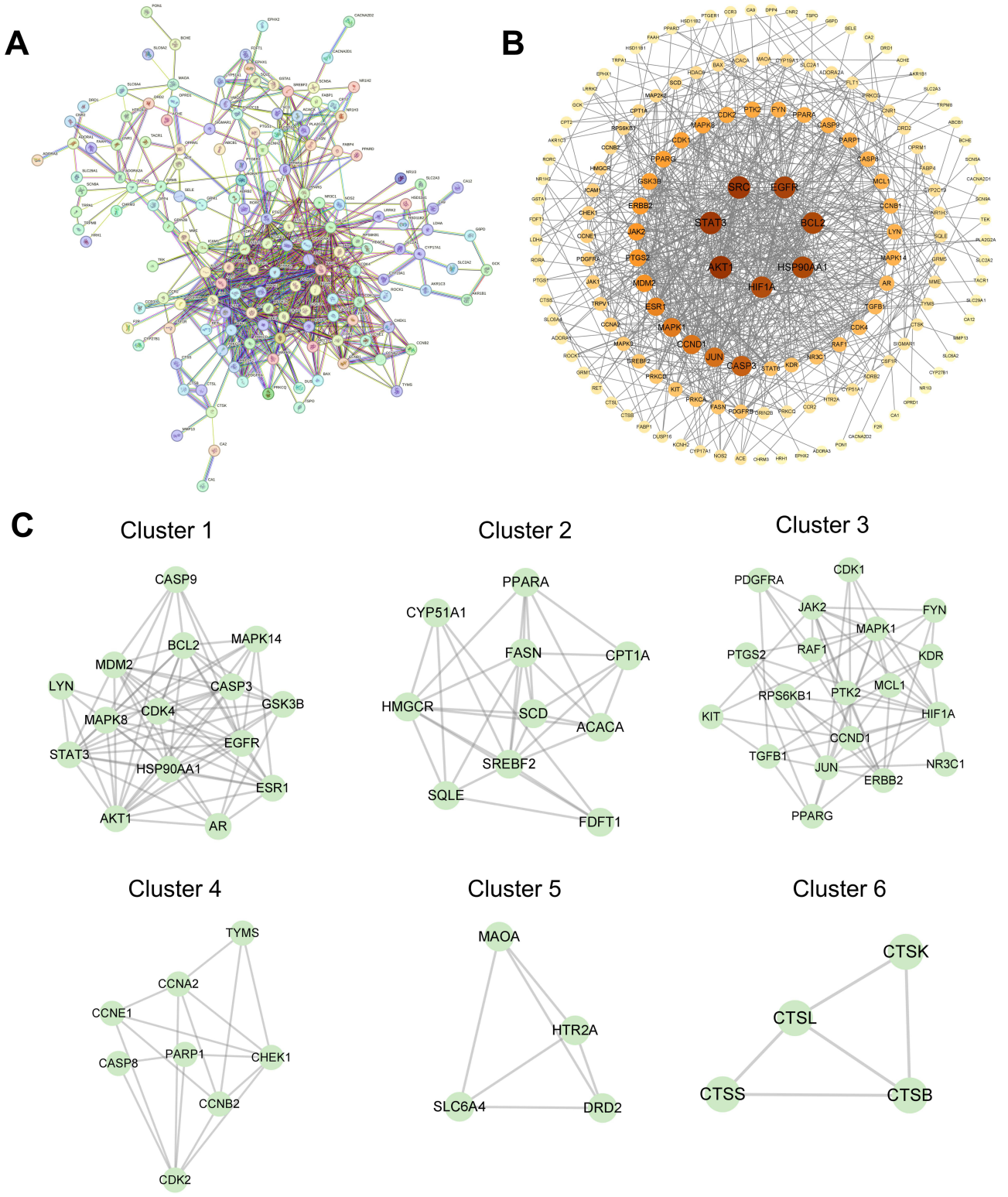

Figure 3 PPI network construction and analysis of the target of LCH treatment for NP. (**A**) PPI network diagram of the target of LCH treatment of NP. (**B**) Topological analysis of the PPI network using CytoNCA plug-in in Cytoscape 3.9.0 software. The node size indicates the degree value. The darker the node color, the larger is the degree value. (**C**) Cluster analysis of PPI network.

Table 3 Clusters of Target Genes of Ligusticum Chuanxiong Hort Against Neuropathic Pain

Cluster	Score (Density Nodes)	Nodes	Edges	Node IDs
1	10	15	70	GSK3B, ESR1, CASP3, AR, STAT3, MDM2, BCL2, HSP90AA1, AKT1, CDK4, CASP9, MAPK8, LYN, MAPK14, EGFR
2	6.667	10	30	CPT1A, FASN, PPARA, ACACA, HMGCR, SCD, SQLE, CYP51A1, SREBF2, FDFT1
3	6.333	19	57	NR3C1, CCND1, CDK1, RPS6KB1, PDGFRA, RAF1, FYN, PPARG, KDR, TGFB1, PTK2, JUN, MAPK1, MCL1, HIF1A, KIT, PTGS2, ERBB2, JAK2
4	4.857	8	17	PARP1, TYMS, CCNA2, CHEK1, CASP8, CCNB2, CDK2, CCNE1
5	4	4	6	SLC6A4, DRD2, HTR2A, MAOA
6	3.333	4	5	CTSL, CTSK, CTSB, CTSS

pathways, involving a total of 29 target genes. This suggested that the PI3K-AKT pathway could be modulated by LCH in NP treatment. Analysis using the CytoNCA plug-in showed that targets, such as MAPK1, AKT1, RAF1, MAP2K2, MAPK10, MAPK8, MAPK9, PRKCA, and BAX, were significantly enriched in the top 30 KEGG pathways (Figure 7B).

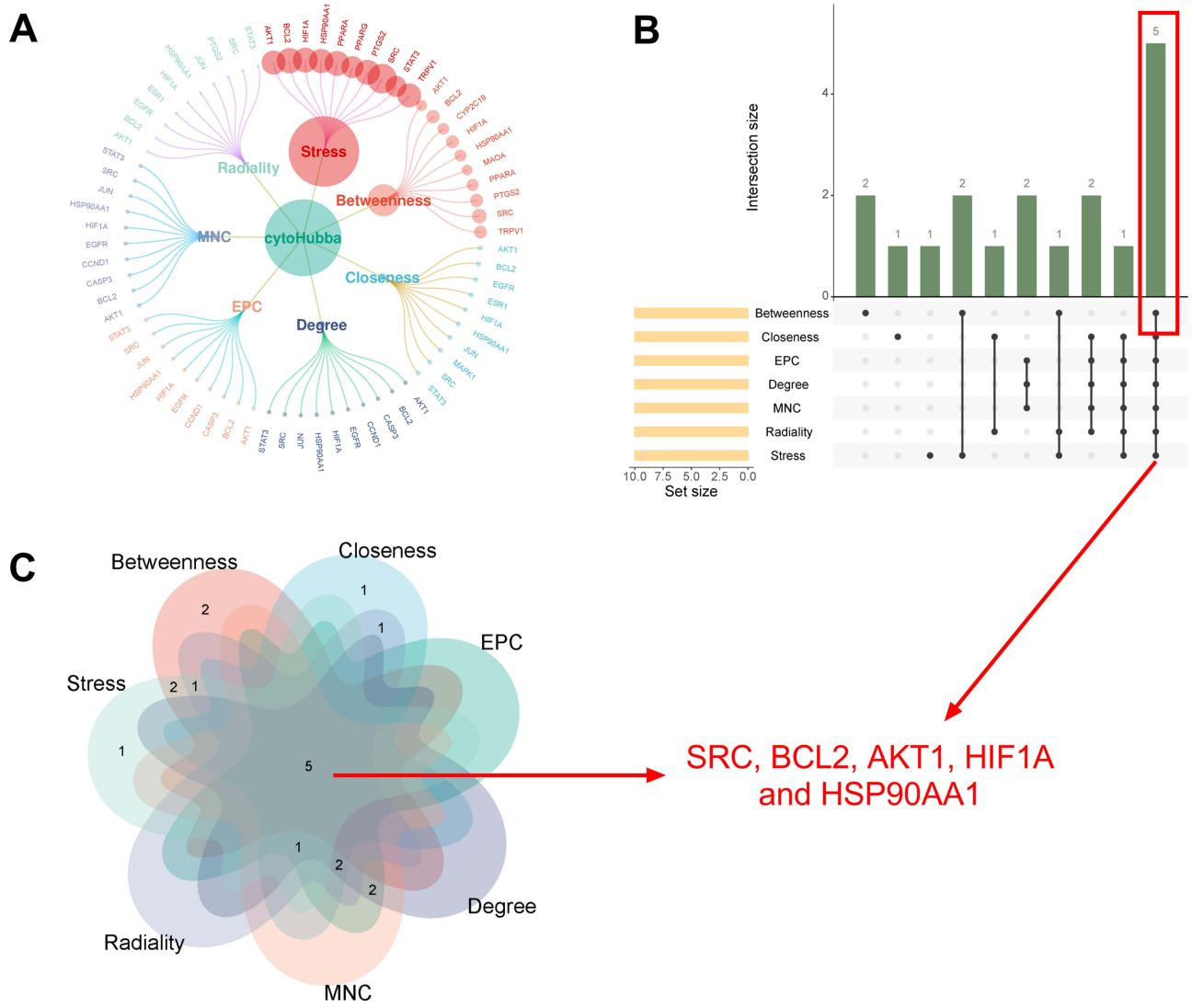

Figure 4 Identification of hub targets. (**A**) R package "ggraph" was applied to visualize the results of the 7 different algorithms of the CytoHubba plugin. (**B**) Seven algorithms (betweenness, closeness, EPC, degree, MNC, radiality and stress) were used to identify hub targets based on R package "UpSet". (**C**) Cross-analyze the results of 7 different algorithms using a Venn diagram.

Table 4 Hub Target Information of Ligusticum Chuanxiong Hort in the Treatment of Neuropathic Pain

NO.	Targets	Uniprot ID	Betweenness	Closeness	EPC	Degree	MNC	Radiality	Stress
1	SRC	P12931	3754.447113	88.38333333	36.47	41	38	7.909090909	20,672
2	BCL2	P10415	2988.800083	84.96666667	36.196	38	34	7.798701299	14,434
3	AKT1	P31749	1679.30727	88.58333333	37.953	42	42	7.876623377	12,814
4	HIF1A	Q16665	2674.148772	86	35.754	37	36	7.837662338	13,842
5	HSP90AA1	P07900	2203.193427	85.45	36.701	38	36	7.785714286	13,104

In addition, PathView was used to stain the targets of the PI3K-AKT signaling pathway, and the targets of LCH in NP treatment are marked in red (Figure 7C).

Results of Molecular Docking

Next, molecular docking was performed to analyze the binding energy of hub proteins to the key components of LCH. Blind docking was performed using the AutoDockTools-1.5.7 software (Table 5). Binding affinity < −4.25 kcal/mol indicates that two molecules have standard binding ability, < −5.0 kcal/mol indicates good binding, and < −7.0 kcal/mol indicates strong binding activity.[22] The binding energy results for the hub target protein and key active components are shown in Figure 8. The binding capacity of β-sitosterol, senkyunone, wallichilide, myricanone and mandenol with SRC, BCL2, AKT1 and HSP90AA1 was less than −5.0 kcal/mol. However, the binding ability of HIF1A is weak (Figure 9). Considering the degree

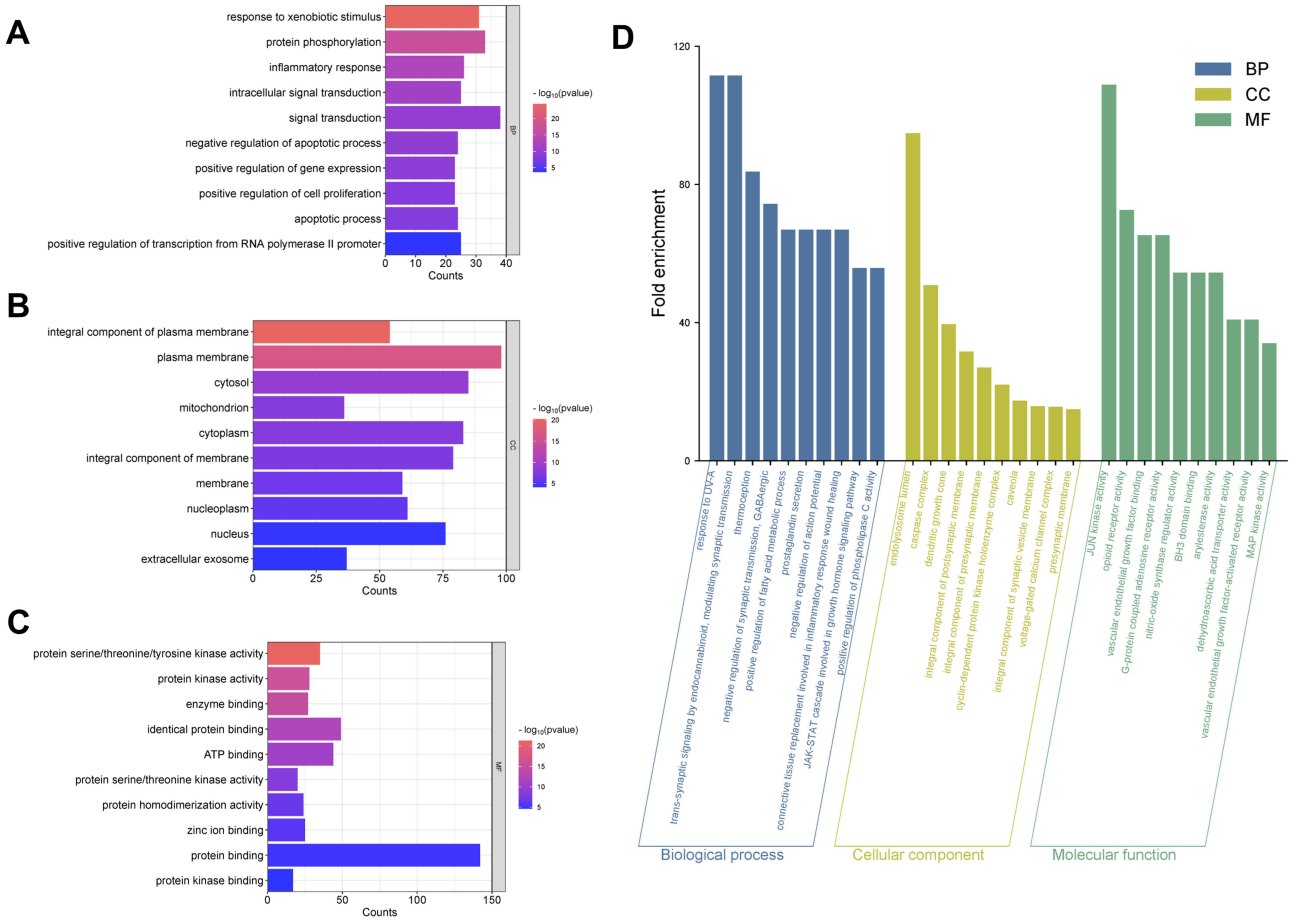

Figure 5 GO functional enrichment analysis of LCH therapeutic targets for NP. (**A**–**C**) BP (**A**), CC (**B**) and MF (**C**) items with the largest number of genes were visualized with bar graphs, with $P < 0.01$ as the screening condition. The vertical and horizontal axes show the items' name and gene counts, respectively. The P values are displayed in different colors. (**D**) Enrichment analysis diagram of BP (blue), CC (yellow) and MF (green) with the top 10 enrichment ratios (P <0.01).

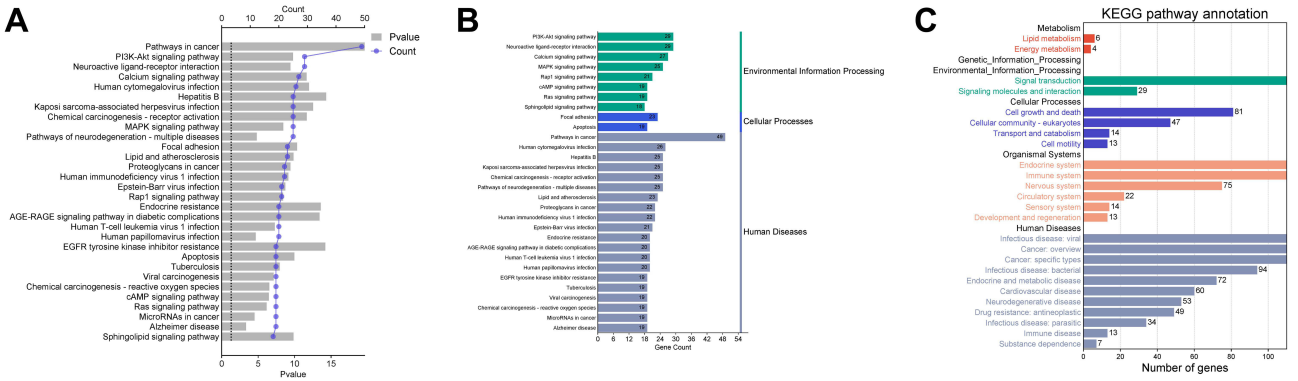

Figure 6 KEGG pathway enrichment analysis of LCH targets for NP. (**A**) The top 30 KEGG pathways with the most gene counts associated with LCH treatment of NP were visualized using double X-axis bar and line plots ($P < 0.01$). The vertical axis represents the term name. The horizontal axis represents gene count and *P*-value respectively. (**B**) Classification summary diagram of the top 30 KEGG pathways. (**C**) Secondary classification of all KEGG pathways.

value of β-sitosterol was the highest among the crucial components of LCH (Figure 2C), and it had higher potential binding affinity with AKT1 (3O96, −11.2 kcal/mol) and SRC (4K11, −8.6 kcal/mol), molecular dynamics simulation was further performed to validate the binding relationship between β-sitosterol and AKT1 and SRC. The RMSD values of β-sitosterol /AKT1 system and β-sitosterol/SRC system increased after the simulation began, and reached states of equilibrium after 30 ns and 6 ns, respectively; the RMSD values of the AKT1 and SRC were higher than those of them in complex systems, indicating a higher stability of the complexes throughout the simulations; additionally, for β-sitosterol/AKT1 system, after equilibrium, the change of RMSD was less than 3.2 Å, also suggesting the binding was stable, and for β-sitosterol/SRC system, the plot showed that RMSD of the protein was below 3.4 Å, which indicated a high binding affinity between β-sitosterol and SRC (Figure 10A and B). RMSF showed that, β-sitosterol had good ability to lower the local fluctuations of residues of AKT1 and SRC (Figure 10C and D). The results of molecular dynamics simulation further supported that β-sitosterol could bind with AKT1 and SRC, and probably suppressed PI3K/AKT signaling.

Effect of β-Sitosterol on LPS-Induced M1 Polarization of Microglia

To verify the potential therapeutic effect of LCH on NP, the active component of LCH with the highest degree value, β-sitosterol, was selected for in vitro study. First, the cytotoxicity of β-sitosterol on microglial HMC3 cells was evaluated at different concentrations (0, 7.5, 15, 30, and 60 μM). The results showed that different concentrations of β-sitosterol did not induce significant cytotoxicity in the HMC3 cells (Figure 11A). Therefore, in subsequent experiments, 30 μM and 60 μM β-sitosterol were used as the medium dose and high dose, respectively, to pre-protect the microglia. To induce M1 polarization of HMC3 cells, the cells were treated with 100 ng/mL LPS for 24 h. qRT-PCR and Western blot were used to detect the effects of β-sitosterol treatment on the mRNA and protein expression levels of M1 polarization-related markers (iNOS, CD86, COX-2, TNF-α, IL-6, IL-1β) in microglia, respectively. The results showed that LPS treatment significantly increased the mRNA and protein expression levels of iNOS, CD86, COX-2, TNF-α, IL-6, and IL-1β in HMC3 cells, and β-sitosterol treatment reversed the effects of LPS (Figure 11B–I). ELISA results showed that β-sitosterol reduced the increase in TNF-α, IL-6 and IL-1β levels in LPS-induced HMC3 cells in a dose-dependent manner (Figure 11J–L). Taken together, these data suggest that β-sitosterol suppresses M1 polarization and expression of pro-inflammatory factors in microglia.

β-Sitosterol Treats NP by Regulating the Expression of Hub Targets and Inhibiting PI3K-Akt Signaling Pathway

Network pharmacological analysis suggested that LCH might treat NP by acting on hub targets such as SRC, BCL2, AKT1, and HSP90AA1, and regulating the PI3K-Akt pathway. To verify the results of network pharmacology, qRT-PCR was performed to detect the effect of β-sitosterol on the mRNA expression levels of hub targets. The results showed that β-sitosterol reduced LPS-induced up-regulation of SRC, BCL2, AKT1, and HSP90AA1 mRNA expression levels in

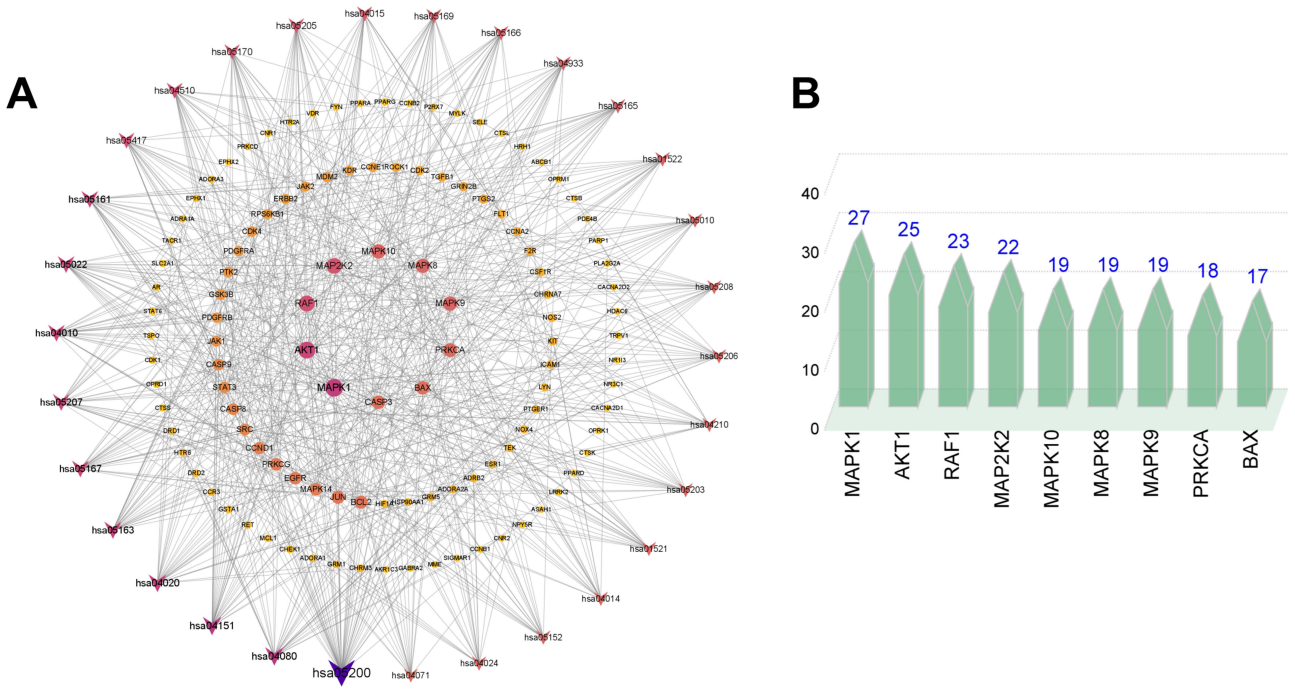

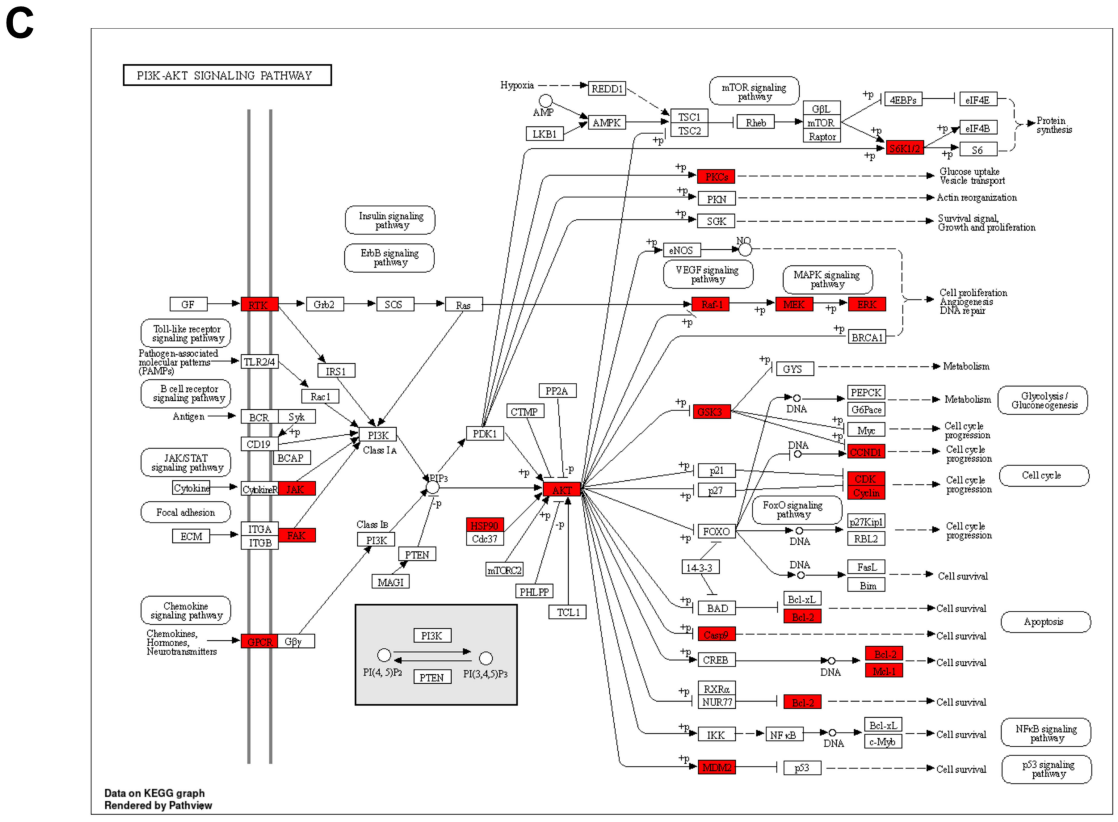

Figure 7 Construction and analysis of the top 30 KEGG pathway-target networks. (**A**) Pathway-target network diagram was constructed using Cytoscape 3.9.0 software. V-shaped nodes represent pathways, and circular nodes represent targets. The node size or color shade is proportional to degree value. (**B**) Degree value statistics of the top 9 targets in the pathway-target network. (**C**) Distribution of key targets in PI3K /AKT signaling pathway.

https://doi.org/10.2147/JPR.S446137 DovePress

Table 5 Docking Center and Binding Pocket of Compounds and Targets

Targets (PDB ID)	Compounds	Docking Center (x, y, z)	Docking Pocket (x, y, z)
SRC (4K11)	β-sitosterol, Senkyunone, Wallichilide, Myricanone and Mandenol	x = 21.213, y = 34.787, z = 66.465	x = 66.0, y = 68.0, z = 64.0
BCL2 (6GL8)	β-sitosterol, Senkyunone, Wallichilide, Myricanone and Mandenol	x = 4.544, y = 2.356, z = 10.126	x = 42.6, y = 37.8666666667, z = 42.6
AKT1 (3O96)	β-sitosterol, Senkyunone, Wallichilide, Myricanone and Mandenol	x = 6.614, y = −11.218, z = 19.731	x = 54.2888888889, y = 62.0444444444, z = 63.9833333333
HIF1A (3HQR)	β-sitosterol, Senkyunone, Wallichilide, Myricanone and Mandenol	x = 23.967, y = −0.06, z = −15.345	x = 25.1777777778, y = 36.05, z = 20.0277777778
HSP90AA1 (4BQG)	β-sitosterol, Senkyunone, Wallichilide, Myricanone and Mandenol	x = 1.382, y = 16.173, z = 20.571	x = 46.6, y = 46.6, z = 46.6

a dose-dependent manner (Figure 12A–D). Consistently, Western blot analysis showed that LPS stimulation significantly increased protein levels of p-AKT, p-PI3K p85α, and p-mTOR in HMC3 cells, while β-sitosterol treatment significantly reversed this effect (Figure 12E and F). These results indicated that LCH and β-sitosterol could probably exert analgesic effects modulating the phenotype of microglial via PI3K/AKT pathway.

Discussion

The etiology of NP is diverse, and its pathogenesis is complex, and it is related to neuroinflammation after nerve injury.[23] Previous studies have shown that the bioactive components of plants may help treat human diseases, and some monomers and compounds of traditional Chinese herbal medicines can ameliorate NP.[24,25] For example, curcumin reduces

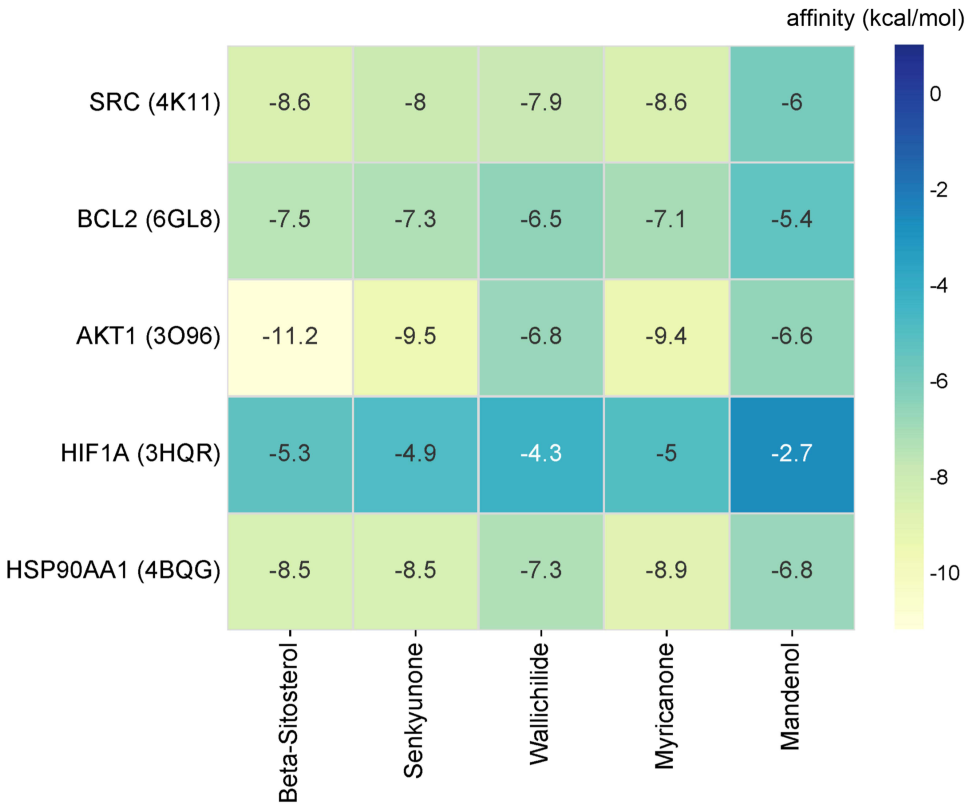

Figure 8 The binding affinity of β-sitosterol, senkyunone, wallichilide, myricanone, mandenol and hub targets SRC (PDB ID: 4K11), BCL2 (PDB ID: 6GL8), AKT1 (PDB ID: 3O96), HIF1A (PDB ID: 3HQR), HSP90AA1 (PDB ID: 4BQG) was visualized with heat maps.

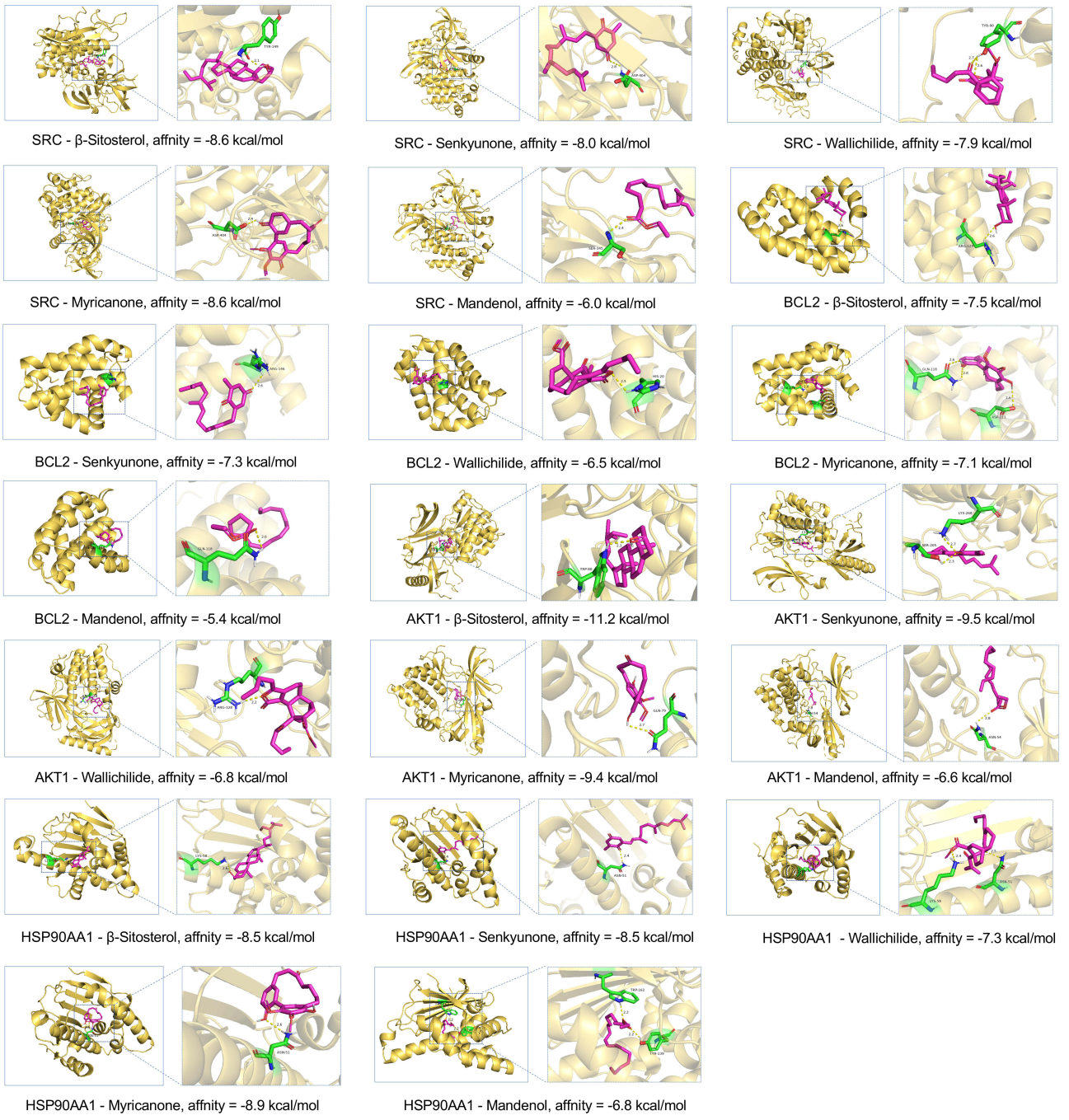

Figure 9 3D molecular docking diagram of key components and hub targets. Purple represents key components (ligands), green represents amino acid residues surrounding the binding bag, and yellow dashed lines represent hydrogen bonds.

neuroinflammation by inhibiting oxidative stress-mediated nuclear factor κB (NF-κB) activation, thereby reducing peripheral neuropathic pain.[25] Network pharmacology is a useful tool to reveal the mechanism of TCM in treating diseases.[26] Through network pharmacology, researchers have found that Duhuo Jisheng decoction, Yuanhu Zhitong Formula, and Gelsemium elegans can treat NP through multi-components, multi-targets, and multi-pathways.[27–29] This study used network pharmacology to explore the potential analgesic mechanisms of LCH and verified these mechanisms using molecular docking techniques and in vitro experiments.

We found that LCH contained at least seven active components, corresponding to 387 targets, of which 178 targets overlapped with NP-associated genes. β-sitosterol, senkyunone, wallichilide, myricanone, and mandenol were found to

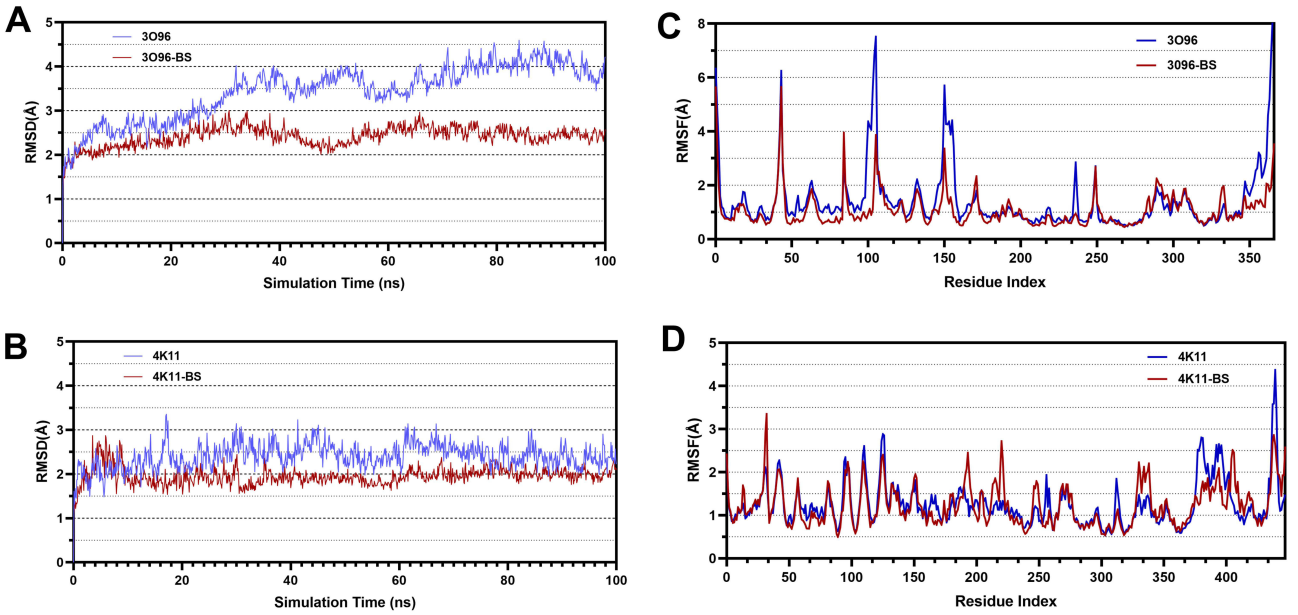

Figure 10 Molecular dynamics simulation suggests β-sitosterol had good binding affinity with AKT1 and SRC. (**A** and **B**). Evolution of RMSDs during 100 ns molecular dynamics simulations of β-sitosterol/AKT1 complex (**A**) and β-sitosterol/SRC complex (**B**). (**C** and **D**) RMSFs of the backbones in β-sitosterol/AKT1 complex (**C**) and β-sitosterol/SRC complex (**D**).

be significantly associated with NP disease targets. Among them, the degree of β-sitosterol was the highest, indicating that it is more likely to play a role in the LCH treatment of NP. Previous studies have shown that β-sitosterol exerts anti-inflammatory and cholesterol-lowering effects.[30] It can also reduce the severity of NP in diabetic mice.[31] For these reasons, in the present work β-sitosterol was selected to explore the potential analgesic mechanism of LCH. In addition, the PPI network showed that LCH ameliorated NP via a complex molecular network. Targets with high topological parameters, such as SRC, BCL2, AKT1, HIF1A, and HSP90AA1, were defined as hub targets. SRC inhibition has been reported to play a protective role in a mouse model with NP by reducing microglia-induced neuroinflammation.[32] BCL2 is an anti-apoptotic protein that plays a key role in apoptosis regulation.[33] Ajugarin-I inhibits vincristine-induced NP by modulating Nrf2/NF-κB and BCL2 signaling.[34] AKT is a key downstream substrate of the PI3K pathway and is involved in various biological processes.[35] It is reported that, activation of PI3K/AKT pathway in spinal cord contributes to activation of the transcription factor NF-κB and release of inflammatory mediators, ultimately leading to the development of NP.[36] Interestingly, this study found that β-sitosterol, senkyunone, wallichilide, myricanone, and mandenol have strong binding activities with SRC, BCL2, AKT1, and HSP90AA1. This suggested that LCH may treat NP by blocking the biological functions of these proteins and their corresponding downstream pathways.

In addition, the results of network pharmacological analysis suggested that LCH may affect NP by controlling large amounts of BP, CC, and MF. Importantly, we found that the targets of LCH are involved in inflammatory response and regulating PI3K/AKT pathway. Several studies have shown that neuroinflammation caused by microglia is closely related to NP.[37] In different microenvironments, activated microglia can manifest as "classically activated" pro-inflammatory M1 type and "vicarious activated" anti-inflammatory M2 type.[38] In the early stages of neuroinflammation, factors secreted by activated microglia affect M1 polarization through autocrine signaling (IL-6, IL-1β and TNF-α), thereby causing pain symptoms.[39] Notably, KEGG enrichment analysis indicated that LCH in NP treatment involves several signaling pathways related to neuroinflammation, such as the PI3K-Akt and MAPK signaling pathways.[40] Among them, the PI3K-Akt signaling pathway is considered to be the core pathway for LCH treatment of NP. Previous studies have shown that TREM2 can improve neuroinflammatory response and cognitive impairment in Alzheimer's disease by regulating PI3K/AKT/FoxO3a signaling pathway.[41] Kurarinone changes M1/M2 polarization of microglia by regulating the IGF1/PI3K/Akt pathway, thereby alleviating heme-induced neuroinflammation and microglia-mediated neurotoxicity.[42] Based on our findings and the results of previous studies, we supposed that LCH may play a therapeutic role by modulating

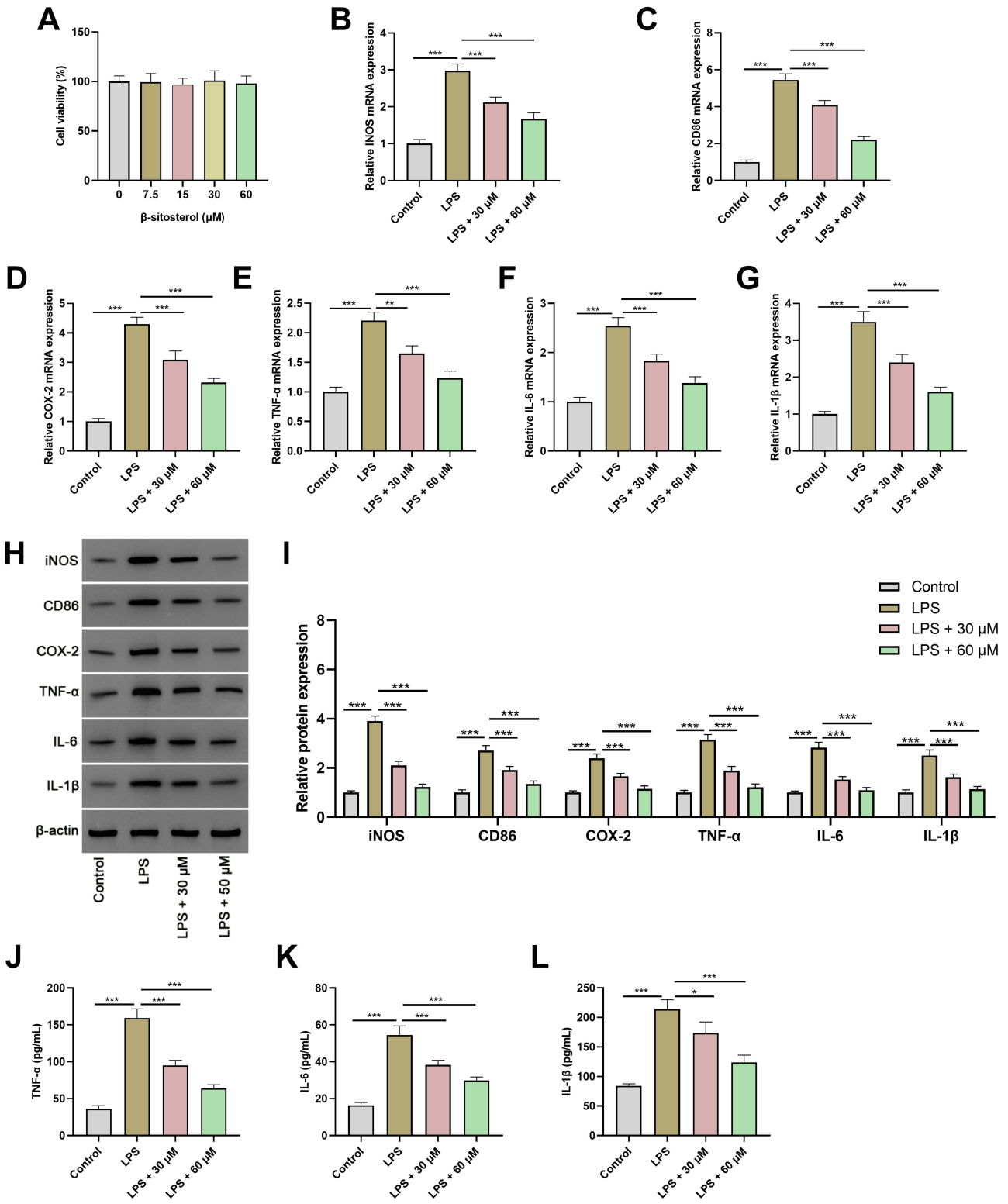

Figure 11 β-sitosterol inhibits LPS-induced M1 polarization of microglia. (**A**) The effects of β-sitosterol at different concentrations (0, 7.5, 15, 30, and 60 μM) on HMC3 cell viability were evaluated using a CCK-8 assay. (**B**–**G**) After HMC3 cells were treated with different concentrations (30 and 60 μM) of β-sitosterol and/or 100 ng/mL LPS for 24 h, the mRNA expression levels of iNOS (**B**), CD86 (**C**), COX-2 (**D**), TNF-α (**E**), IL-6 (**F**), and IL-1β (**G**) were detected by qRT-PCR. (**H** and **I**) The protein levels of iNOS, CD86, COX-2, TNF-α, IL-6 and IL-1β in HMC3 cells treated with β-sitosterol (30 and 60μM) and/or 100ng/mL LPS were detected by Western blot. (**J**–**L**) The levels of TNF-α (**J**), IL-6 (**K**) and IL-1β (**L**) in the supernatants of HMC3 cells were detected by ELISA. **P*<0.05, ***P*<0.01, ****P*<0.001.

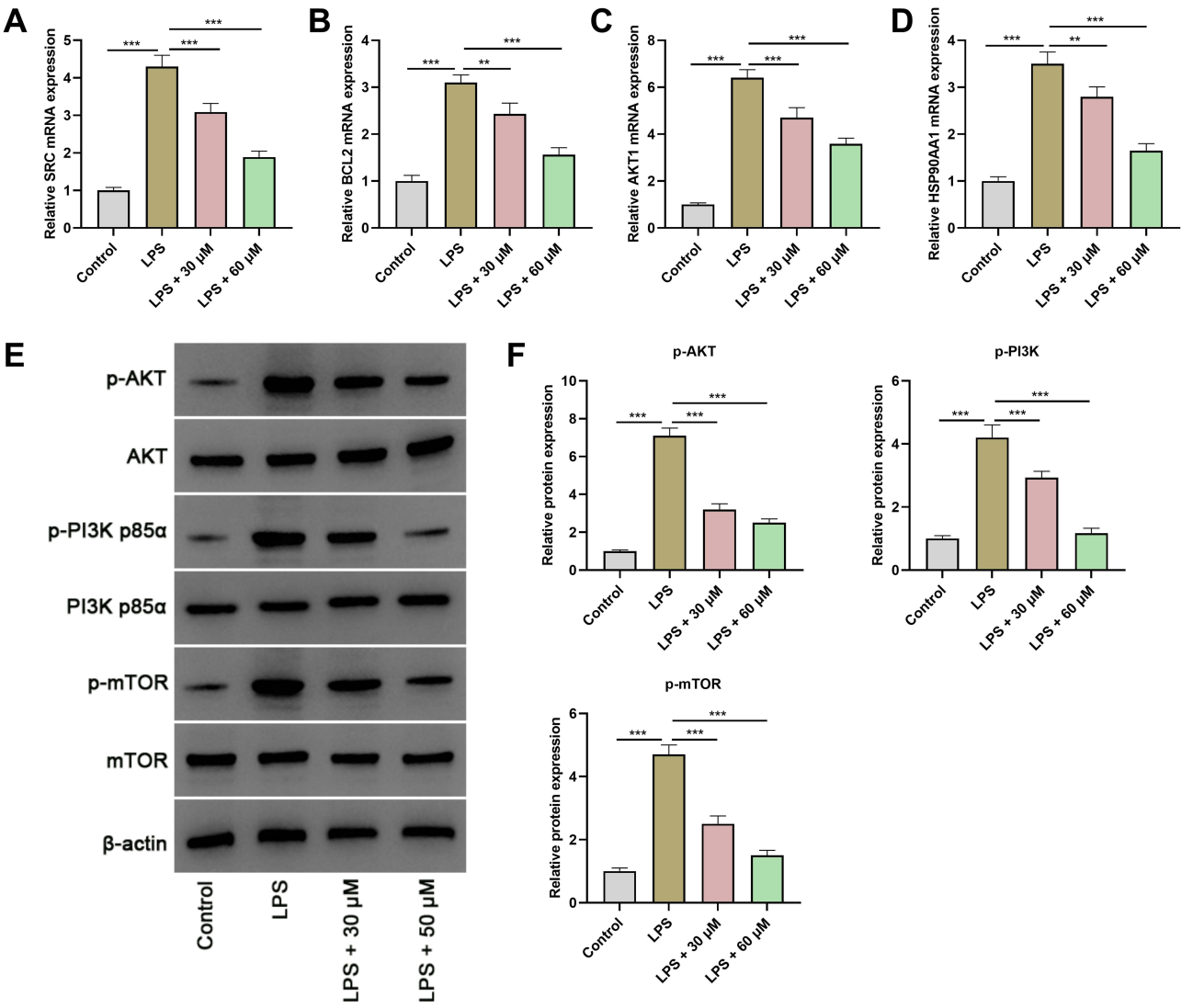

Figure 12 β-sitosterol may exert analgesic effects by regulating the expression of hub targets and the PI3K-Akt signaling pathway. (**A**–**D**) mRNA expression levels of SRC (**A**), BCL2 (**B**), AKT1 (**C**), and HSP90AA1 (**D**) in HMC3 cells treated with different concentrations (30 and 60μM) of β-sitosterol and/or 100ng/mL LPS were detected by qRT-PCR. (**E** and **F**) Protein expression levels of p-AKT, p-PI3K p85α, and p-mTOR in HMC3 cells treated with different concentrations (30 and 60μM) of β-sitosterol and/or 100ng/mL LPS were detected by Western blot. ***P*<0.01, ****P*<0.001.

neuroinflammation, probably via PI3K/Akt signaling. It has been reported that microglia can be activated into the M1 type by LPS stimulation.[21] iNOS, COX2 and CD86 are markers of M1 polarization in microglia and are highly expressed in LPS-stimulated microglia.[43] Interestingly, this study found that LPS stimulation increased the mRNA and protein expression levels of iNOS, CD86, COX-2, TNF-α, IL-6, and IL-1β in microglia, and promoted the secretion of IL-6, IL-1β, and TNF-α, whereas β-sitosterol treatment reversed this effect. In addition, β-sitosterol treatment could reduce the mRNA expression of SRC, BCL2, AKT1 and HSP90AA1 in LPS-induced microglia and inhibit the activation of PI3K-Akt signaling pathway. Taken together, these findings suggest that β-sitosterol may inhibit LPS-induced M1 polarization and inflammation in microglia by regulating the expression of SRC, BCL2, AKT1, HSP90AA1 and the PI3K-Akt signaling pathway, in turn ameliorate NP.

However, this study had some limitations. The reliability of our findings must be verified using in vivo experiments. Secondly, although β-sitosterol is a key active component of LCH, it still cannot fully represent its pharmacological activity, and other active components need to be verified in the future. In addition, it has been found that the interaction

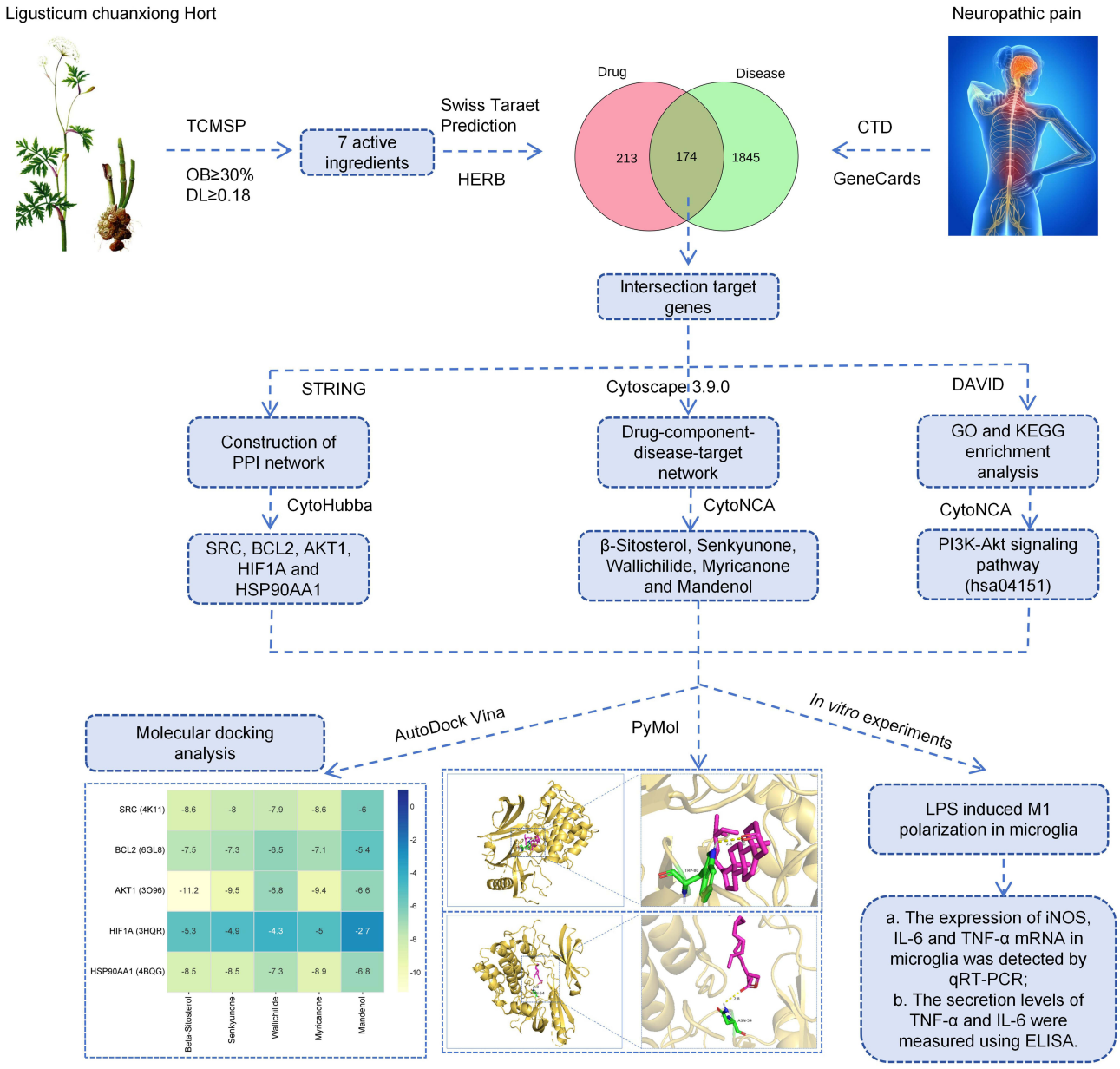

Figure 13 The flow chart of this study.

between astrocytes and microglia is particularly important for the treatment of NP.[44] However, we only examined the changes in microglia. The effects of LCH on astrocytes should be verified in future studies.

Conclusion

This study systematically analyzed the potential mechanism of LCH in attenuating NP and found that β-sitosterol, senkyunone, wallichilide, myricanone, and mandenol are the key chemical components of LCH. SRC, BCL2, AKT1 and HSP90AA1 were hub targets (Figure 13). In vitro studies suggest that β-sitosterol can inhibit LPS-induced M1 polarization of microglia and play an anti-inflammatory role. This study provides a theoretical foundation for the application of LCH in the treatment of NP.

Data Sharing Statement

The data used to support the findings of this study are available from the corresponding author upon request.

Author Contributions

All authors made a significant contribution to the work reported, whether that is in the conception, study design, execution, acquisition of data, analysis and interpretation, or in all these areas; took part in drafting, revising or critically reviewing the article; gave final approval of the version to be published; have agreed on the journal to which the article has been submitted; and agree to be accountable for all aspects of the work.

Funding

This study is supported by the Natural Science Foundation of Hubei Province (Approval No. 2021CFB087).

Disclosure

The authors report no conflicts of interest in this work.

References

1. Scholz J, Finnerup NB, Attal N, et al.; Classification Committee of the Neuropathic Pain Special Interest Group (NeuPSIG). The IASP classification of chronic pain for ICD-11: chronic neuropathic pain. *Pain*. 2019;160(1):53–59. doi:10.1097/j.pain.0000000000001365
2. Finnerup NB, Kuner R, Jensen TS. Neuropathic pain: from mechanisms to treatment. *Physiol Rev*. 2021;101(1):259–301. doi:10.1152/physrev.00045.2019
3. Chen R, Yin C, Fang J, Liu B. The NLRP3 inflammasome: an emerging therapeutic target for chronic pain. *J Neuroinflammation*. 2021;18(1):84. doi:10.1186/s12974-021-02131-0
4. Dydyk AM, Conermann T. *Chronic Pain*. Treasure Island (FL): In StatPearls; 2020.
5. Curtis AF, Miller MB, Rathinakumar H, et al. Opioid use, pain intensity, age, and sleep architecture in patients with fibromyalgia and insomnia. *Pain*. 2019;160(9):2086–2092. doi:10.1097/j.pain.0000000000001600
6. Jiang BC, Liu T, Gao YJ. Chemokines in chronic pain: cellular and molecular mechanisms and therapeutic potential. *Pharmacol Ther*. 2020;212:107581. doi:10.1016/j.pharmthera.2020.107581
7. Ma L, Li J, Zhou J, et al. Intravenous lidocaine alleviates postherpetic neuralgia in rats via regulation of neuroinflammation of microglia and astrocytes. *iScience*. 2021;24(2):102108. doi:10.1016/j.isci.2021.102108
8. Chen H, Zhao Y, Qin G, et al. Antifungal effects and active components of Ligusticum chuanxiong. *Molecules*. 2022;27(14):4589. doi:10.3390/molecules27144589
9. Chen Z, Zhang C, Gao F, et al. A systematic review on the rhizome of Ligusticum chuanxiong Hort. (Chuanxiong). *Food Chem Toxicol*. 2018;119:309–325. doi:10.1016/j.fct.2018.02.050
10. Wang M, Yao M, Liu J, et al. Ligusticum chuanxiong exerts neuroprotection by promoting adult neurogenesis and inhibiting inflammation in the hippocampus of ME cerebral ischemia rats. *J Ethnopharmacol*. 2020;249:112385. doi:10.1016/j.jep.2019.112385
11. Pu ZH, Peng C, Xie XF, et al. Alkaloids from the rhizomes of Ligusticum striatum exert antimigraine effects through regulating 5-HT1B receptor and c-Jun. *J Ethnopharmacol*. 2019;237:39–46. doi:10.1016/j.jep.2019.03.026
12. Chen H, Chen X, Ping Z, et al. Ligusticum chuanxiong promotes the angiogenesis of preovulatory follicles (F1-F3) in late-phase laying hens. *Poult Sci*. 2023;102(3):102430. doi:10.1016/j.psj.2022.102430
13. Yuan X, Han B, Feng ZM, Jiang JS, Yang YN, Zhang PC. Chemical constituents of Ligusticum chuanxiong and their anti-inflammation and hepatoprotective activities. *Bioorg Chem*. 2020;101:104016. doi:10.1016/j.bioorg.2020.104016
14. Xiang C, Liao Y, Chen Z, et al. Network Pharmacology and Molecular Docking to Elucidate the Potential Mechanism of Ligusticum Chuanxiong Against Osteoarthritis. *Front Pharmacol*. 2022;13:854215. doi:10.3389/fphar.2022.854215
15. Du JC, Xie XF, Xiong L, Sun C, Peng C. 川芎挥发油的化学成分与药理活性研究进展 [Research progress of chemical constituents and pharmacological activities of essential oil of Ligusticum chuanxiong]. *Zhongguo Zhong Yao Za Zhi*. 2016;41(23):4328–4333. Chinese. doi:10.4268/cjcmm20162306
16. Du DD, Zhang MY, Liu Y, et al. 川芎干预Panx1-Src-NMDAR-2B信号通路对神经病理性疼痛模型大鼠中枢敏化的作用机制研究 [Mechanism of Chuanxiong Rhizoma intervention on central sensitization of Panx1-Src-NMDAR-2B signaling pathway in neuropathic pain model rats]. *Zhongguo Zhong Yao Za Zhi*. 2021;46(16):4175–4186. Chinese. doi:10.19540/j.cnki.cjcmm.20210513.401
17. Tao B, Wang Q, Cao J, et al. The mechanisms of Chuanxiong Rhizoma in treating spinal cord injury based on network pharmacology and experimental verification. *Ann Transl Med*. 2021;9(14):1145. doi:10.21037/atm-21-2529
18. Wang W, Xu L, Zhou L, Wan S, Jiang L. A network pharmacology approach to reveal the underlying mechanisms of rhizoma dioscoreae nipponicae in the treatment of asthma. *Evid Based Complement Alternat Med*. 2022;2022:4749613. doi:10.1155/2022/4749613
19. Luo Y, Fu Y, Tan T, et al. Screening of lncRNA-miRNA-mRNA coexpression regulatory networks involved in acute traumatic coagulation dysfunction based on CTD, GeneCards, and PharmGKB databases. *Oxid Med Cell Longev*. 2022;2022:7280312.
20. Yang J, Wang C, Cheng S, et al. Construction and validation of a novel ferroptosis-related signature for evaluating prognosis and immune microenvironment in ovarian cancer. *Front Genet*. 2023;13:1094474. doi:10.3389/fgene.2022.1094474
21. Yuan J, Fei Y. Lidocaine ameliorates chronic constriction injury-induced neuropathic pain through regulating M1/M2 microglia polarization. *Open Med*. 2022;17(1):897–906. doi:10.1515/med-2022-0480
22. Saikia S, Bordoloi M. Molecular docking: challenges, advances and its use in drug discovery perspective. *Curr Drug Targets*. 2019;20(5):501–521. doi:10.2174/1389450119666181022153016
23. Austin PJ, Moalem-Taylor G. The neuro-immune balance in neuropathic pain: involvement of inflammatory immune cells, immune-like glial cells and cytokines. *J Neuroimmunol*. 2010;229(1–2):26–50. doi:10.1016/j.jneuroim.2010.08.013

24. Abhishek B, Chattopadhyay RR. Isolation, identification and chemical characterization of compounds from phenolic extracts of peels of kufri chipsona-3 and kufri jyoti potatoes having synergistic antioxidant interactions in combination. *J Food Nutrit Diet Sci*. 2024;2(1):29–40.
25. Zhang X, Guan Z, Wang X, et al. Curcumin alleviates oxaliplatin-induced peripheral neuropathic pain through inhibiting oxidative stress-mediated activation of NF-κB and mitigating inflammation. *Biol Pharm Bull*. 2020;43(2):348–355. doi:10.1248/bpb.b19-00862
26. Zhang R, Zhu X, Bai H, Ning K. Network pharmacology databases for traditional Chinese medicine: review and assessment. *Front Pharmacol*. 2019;10:123. doi:10.3389/fphar.2019.00123
27. Gao C, Zhao Y, Yang T, Gao X, Meng C. Duhuo Jisheng decoction alleviates neuroinflammation and neuropathic pain by suppressing microglial M1 polarization: a network pharmacology research. *J Orthop Surg Res*. 2023;18(1):629. doi:10.1186/s13018-023-04121-9
28. Liu T, Li T, Chen X, et al. A network-based analysis and experimental validation of traditional Chinese medicine Yuanhu Zhitong Formula in treating neuropathic pain. *J Ethnopharmacol*. 2021;274:114037. doi:10.1016/j.jep.2021.114037
29. Que W, Wu Z, Chen M, et al. Molecular mechanism of Gelsemium elegans (Gardner and Champ.) Benth. Against neuropathic pain based on network pharmacology and experimental evidence. *Front Pharmacol*. 2022;12:792932.
30. Shen CY, Lee CF, Chou WT, Hwang JJ, Tyan YS, Chuang HY. Liposomal β-sitosterol suppresses metastasis of CT26/luc colon carcinoma via inhibition of MMP-9 and evoke of immune system. *Pharmaceutics*. 2022;14(6):1214. doi:10.3390/pharmaceutics14061214
31. Raafat K, Hdaib F. Neuroprotective effects of Moringa oleifera: bio-guided GC-MS identification of active compounds in diabetic neuropathic pain model. *Chin J Integr Med*. 2017. doi:10.1007/s11655-017-2758-4
32. Cai Y, Xu J, Cheng Q. Proto-oncogene tyrosine-protein kinase SRC (Src) inhibition in microglia relieves neuroinflammation in neuropathic pain mouse models. *Bioengineered*. 2021;12(2):11390–11398. doi:10.1080/21655979.2021.2008694
33. Eom YH, Kim HS, Lee A, Song BJ, Chae BJ. BCL2 as a subtype-specific prognostic marker for breast cancer. *J Breast Cancer*. 2016;19 (3):252–260. doi:10.4048/jbc.2016.19.3.252
34. Khan A, Shal B, Ullah khan A, et al. Neuroprotective mechanism of Ajugarin-I against Vincristine-Induced neuropathic pain via regulation of Nrf2/NF-κB and Bcl2 signalling. *Int Immunopharmacol*. 2023;118:110046. doi:10.1016/j.intimp.2023.110046
35. Okerman T, Jurgenson T, Moore M, Klein AH. Inhibition of the phosphoinositide 3-kinase-AKT-cyclic GMP-c-Jun N-terminal kinase signaling pathway attenuates the development of morphine tolerance in a mouse model of neuropathic pain. *Mol Pain*. 2021;17:17448069211003375. doi:10.1177/17448069211003375
36. Chen SP, Zhou YQ, Liu DQ, et al. PI3K/Akt pathway: a potential therapeutic target for chronic pain. *Curr Pharm Des*. 2017;23(12):1860–1868. doi:10.2174/1381612823666170210150147
37. Guan Z, Kuhn JA, Wang X, et al. Injured sensory neuron-derived CSF1 induces microglial proliferation and DAP12-dependent pain. *Nat Neurosci*. 2016;19(1):94–101. doi:10.1038/nn.4189
38. Piotrowska A, Kwiatkowski K, Rojewska E, Makuch W, Mika J. Maraviroc reduces neuropathic pain through polarization of microglia and astroglia - Evidence from in vivo and in vitro studies. *Neuropharmacology*. 2016;108:207–219.
39. Wu J, Ding DH, Li QQ, Wang XY, Sun YY, Li LJ. Lipoxin A4 Regulates Lipopolysaccharide-Induced BV2 Microglial Activation and Differentiation via the Notch Signaling Pathway. *Front Cell Neurosci*. 2019;13:19. doi:10.3389/fncel.2019.00019
40. Liu B, Zhang Y, Yang Z, et al. ω-3 DPA protected neurons from neuroinflammation by balancing microglia M1/M2 polarizations through inhibiting NF-κB/MAPK p38 SIGNALING AND ACTIVATING NEuron-BDNF-PI3K/AKT pathways. *Mar Drugs*. 2021;19(11):587. doi:10.3390/md19110587
41. Wang Y, Lin Y, Wang L, et al. TREM2 ameliorates neuroinflammatory response and cognitive impairment via PI3K/AKT/FoxO3a signaling pathway in Alzheimer's disease mice. *Aging*. 2020;12(20):20862–20879. doi:10.18632/aging.104104
42. Jia ZQ, Zuo C, Yue WF. Kurarinone alleviates hemin-induced neuroinflammation and microglia-mediated neurotoxicity by shifting microglial M1/M2 polarization via regulating the IGF1/PI3K/Akt signaling. *Kaohsiung J Med Sci*. 2022;38(12):1213–1223. doi:10.1002/kjm2.12597
43. Jiang Q, Wei D, He X, Gan C, Long X, Zhang H. Phillyrin prevents neuroinflammation-induced blood-brain barrier damage following traumatic brain injury via altering microglial polarization. *Front Pharmacol*. 2021;12:719823. doi:10.3389/fphar.2021.719823
44. Linnerbauer M, Wheeler MA, Quintana FJ. Astrocyte Crosstalk in CNS Inflammation. *Neuron*. 2020;108(4):608–622. doi:10.1016/j.neuron.2020.08.012